

Status of the LHCb experiment

CERN-RRB-2019-037

17 April 2019

1 Introduction

The 2018 proton-proton run ended successfully in October 2018 with a record luminosity of 2.5 fb^{-1} delivered and 2.2 fb^{-1} collected by LHCb. A total of 10 fb^{-1} were delivered to LHCb in Run 1 + Run 2 data taking periods, with 9 fb^{-1} collected by the experiment.

The proton-proton run was followed by an equally successful heavy ion run at $\sqrt{s_{NN}} = 5.02 \text{ TeV}$, with a recorded luminosity of Pb-Pb collisions of about 0.2 nb^{-1} . This is the largest Pb-Pb sample ever collected by LHCb. In addition, a substantial sample of Pb-Ne collisions in fixed target mode has also been collected.

The operational efficiency was 90% and all subdetectors operated in a very stable way. A flexible trigger strategy was in place that allowed LHCb to take data in diverse beam conditions, profiting from all useful luminosity to perform physics studies. More information can be found in Secs. 2 and 3.

The installation activities for the upgrade started immediately at the beginning of LHC Long Shutdown 2 and are now in full swing.

The year 2018 has been highly successful for the LHCb physics output, with 41 papers submitted to journals. In total 466 papers have now been published or submitted.

Physics highlights since the last report include the measurement of the charm-mixing parameter y_{CP} , the reporting of evidence for an $\eta_c(1S)\pi^-$ resonance in $B^0 \rightarrow \eta_c(1S)K^+\pi^-$ decays, the observation of two new resonances in the $\Lambda_b^0\pi^\pm$ systems, the measurement of b -hadron fractions in 13 TeV pp collisions and the first measurement of charm production in fixed-target configuration at the LHC. These and other results are discussed in Sect. 4. Further important results will be presented at the upcoming winter conferences and will be discussed at the time of the RRB meeting.

This is the final operational report for the original LHCb detector. Much of our efforts are invested into preparations for the LHCb Upgrade I, which is now entering the installation phase. This work is described in a separate document [1].

2 Detector sub-systems

The LHCb experiment operated very successfully until the end of Run 2 and only minor issues were reported. For the technical coordination team, the main emphasis was on the preparation of Long-Shutdown 2. Temporary storage areas for the obsolete detector and services are completed and most of the tooling and handling equipment for the detector removal are ready. On day one of LS2 the dismantling of the shielding wall started, and this was completed just before the CERN closure at the end of 2018. Cooling plants that will not be used anymore have been removed from the cavern, as well as optical fibres and a large fraction of copper cables. Furthermore, the Inner and Outer Tracker left the cavern together with the Velo sensors and electronics. The work for LS2 is well on track so far.

2.1 Vertex Locator (VELO)

The VELO detector had an eventful final semester of operations before the end of Run 2 and the start of de-installation. During the technical stop a current scan was performed at varying temperature settings, as part of the ongoing radiation damage studies, and the regular CCE scans were taken during the LHC runs with low numbers of bunches. However a few days later an intervention performed by MOEDAL caused direct damage which could have resulted in significant loss of data and time for the experiment. Various MOEDAL elements were installed directly in the middle of the VELO cable runs without communicating beforehand, which resulted in faulty connections in the VELO readout and controls. Fortunately, the investigation and cure could be carried out largely during the remaining time of the technical stop, minimising the impact. However manpower was diverted from the planned maintenance, including the optimisation of the Beetle chip settings, resulting in a small risk to the detector due to power settings that were slightly higher than necessary.

On 26th Nov 2018 the VELO motion system underwent its first failure in over 10 years of operation. The motion mechanism got stuck during the closing procedure after Stable Beams had been declared. The on-call expert concluded it was a hardware problem which required a hardware intervention by non on-call expertise. The fill was able to continue successfully until 8 am, but after the beam dump the position of the detectors interlocked the injection, preventing the refilling of the LHC. The problem was caused by a faulty power supply that caused a cascade fuse break-down in the mains. The spare power supply was found to have an incompatible part and the sequence of soldering older components onto the power supply board, in addition to tracking down the errors with the fuses, prevented LHC filling for about six and a half hours. After refilling and re-referencing the motion system the VELO closed successfully; the intervention posed no risks at any moment in terms of machine protection.

Despite these events the detector continued to operate with close to design efficiency. The major concern in previous years had been the stability of operation

of the HV power supplies. These had been previously tested and showed signs of intermittent trips of unknown cause. A fault detection and recovery algorithm was installed which operated steadily throughout the year. The bias currents continued to rise as expected and a programmed beneficial annealing of the sensors via a deliberate warm up of the VELO took place in the technical stop in September, which reduced the magnitude of the leakage currents by 10-20% and the effective depletion voltage by about 70-80V, resulting in improved efficiency for the most irradiated detector regions, Fig. 1. We believe this may be the first time beneficial annealing has been intentionally performed on an operational detector. The effects of running the sensors with higher reversed bias voltages was investigated in the very final fill of the LHC in run 2. The VELO HV system had been qualified and tested to operate to up to 500 V, although the supplies could provide 700 V. A special HV scan was planned to reach the maximum possible bias voltage during stable beam operation. The objective was two-fold: the mechanism of thermal runaway (causes and manifestations) was investigated; the effects of operating at a large overvoltage on the detector efficiency and charge collection, Fig. 2. The overdesign value of 700 V was reached for all but two of the sensors and the preliminary analysis is very promising, showing complete recovery of efficiency for the innermost regions at the highest voltage.

The VELO has now been fully de-cabled and the deinstallation of the sensors was performed in week 9 of 2019.

2.2 Silicon Tracker (ST)

The Tracker Turicensis (TT) and Inner Tracker (IT) performed well in their final months of operation in Run 2. The fraction of working channels in the TT and IT remained unchanged for most of 2018, at 98.92% and 98.86%, respectively. Monitoring of the radiation damage in the silicon sensors, performed through continuous leakage current measurements and periodic Charge Collection Efficiency (CCE) scans, showed that both detectors aged as expected through Runs 1 and 2. The detectors will be dismantled during the ongoing long shutdown (LS2).

The problem with desynchronisation errors in the readout electronics of one TT module, reported in the previous RRB document, was investigated during the September 2018 Technical Stop (TS). The errors remained after replacement of both the associated TELL1 and digitizer board, and it was concluded that the problem most likely originated from the backplane of the service box. Since the loss of these readout channels had no impact on data quality, it was decided to forego any intervention on the service boxes.

During the September TS, a search was also performed to identify the IT C_6F_{14} cooling circuit leak responsible for the increased coolant loss rate reported previously; no new leaks were found at the time. After interventions to lower the pressure in the cooling circuit and refill the C_6F_{14} tanks, the loss rate was lowered to just under one litre per day for the last month of data-taking.

The dismantling of the IT commenced on January 29, and is mostly completed

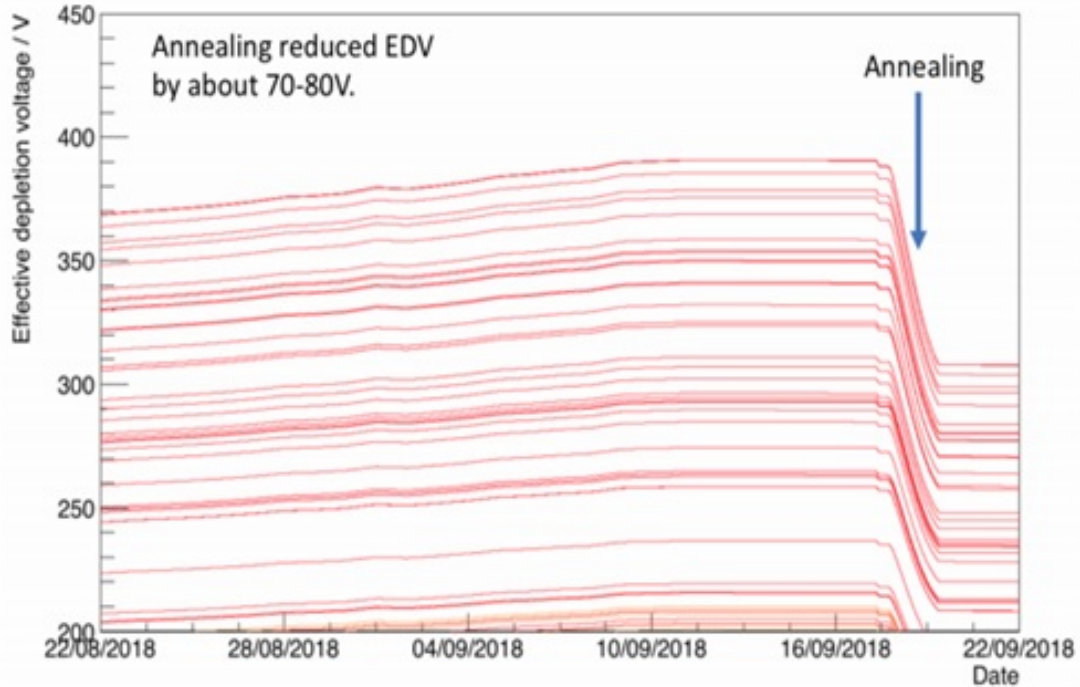


Figure 1: VELO effective depletion voltages as a function of time, illustrating the drop due to the beneficial annealing performed during the last Technical Stop of 2018.

at the time of writing of this document. During the detector dismantling, a probable source of the cooling circuit leak was found to be located within the armaflex of the IT1A half-station. The TT dismantling is scheduled to begin on March 6. A subset of TT modules, IT detector boxes and service boxes will be transported to ST group institutes, primarily for outreach display purposes. The Brandeis CCD Angle Monitor (BCAM) based system, installed during LS1 to monitor the movement of the IT half-stations, will be reused for the upgrade scintillating fibre tracker.

2.3 Outer Tracker (OT)

The Outer Tracker detector (OT) was included in the PbPb run at the end of Run-2 in November and December 2018, marking the end of operation of the OT after about 10 years of successful data taking. A final noise scan was conducted for documentation purposes, and only four modules were found to be noisy, resulting in about 40 noisy channels out of 53760 channels in total. The high occupancy of the OT of about 13% during LHCb operation at instantaneous luminosity values of $4.5 \cdot 10^{32} \text{cm}^{-2} \text{s}^{-1}$ led to large data rates. The OT was limiting the LHCb event

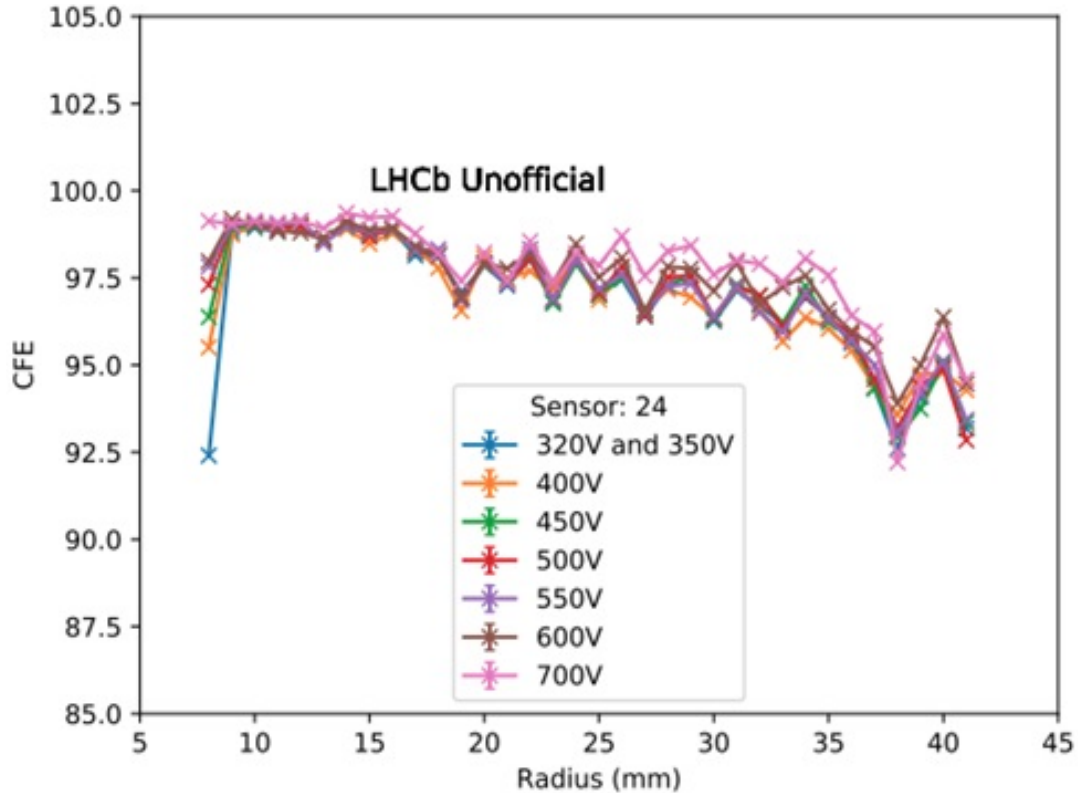


Figure 2: Analysis of the Very High Voltage special scan taken in the last LHC fill. At the highest, over design voltage of 700V, the most irradiated few mm of the inner radius of the detector become fully efficient.

rate to about 950 kHz, but was mitigated by an extra event cut on events where the previous event was particularly busy. This reduced the occupancy of the OT, as the drift times of hits in the OT span more than two bunch crossings.

The OT did not suffer from any significant operational problems during its entire lifetime, and data taking in 2018 went particularly smoothly, including the PbPb run. No sign of performance degradation has been observed, due to radiation damage or otherwise. The Panda experiment has expressed interest in recovering and reusing some of the electronic systems and the central (half) modules. In that context, the Panda collaboration will receive the necessary OT tooling components and all the spare detector modules in early 2019, to study the potential use of parts of the OT in the final PANDA detector.

The dismantling of the OT is already underway; the gas rate was lowered to 300 l/h after the end of the operations in 2018. A complete stop of the gas system can potentially pollute the gas volume in the straws, and hence it was avoided till early February when the detector volume was closed and the C-frames were disconnected (on both the A-Side and C-side). By the beginning of March, the OT

will be removed from the cavern. The final step is to transport the 12 C-frames - with all detector modules and front-end units mounted - in a single steel transport frame. The frame will be transported to the surface, and then transported to the storage building on the Preveessin site for radiation cooldown. At the end of the long shutdown 2, the modules and electronics will be unmounted.

2.4 RICH system

The RICH detectors have worked extremely well in 2018 with no software or hardware issues to report. All the required maintenance took place during the YETS at the end of 2017. No further maintenance (see CERN-RRB-2018-099) was needed before the end of the year and the dismantling of the current detectors. The air contamination of the C_4F_{10} gas in RICH 1 has been followed closely over the years and a procedure for cleaning the gas during a Technical Stop (TS) without first emptying the whole volume was introduced during LS1. Since 2015, pure C_4F_{10} is introduced in RICH 1 at the start of the year and it is cleaned again once during the year when the contamination has reached approximately 1%. The RICH 1 gas was cleaned again during the September 2018 TS. A full Upgrade detector module was installed in RICH 2 and operated in parallel with the LHCb acquisition system using the LHCb trigger decisions. It was possible to detect light synchronous with the LHC collisions and to get valuable experience with the Upgrade DAQ system and operation of the Upgrade front-end electronics.

2.5 Calorimeters (SPD, PS, ECAL and HCAL)

The Calorimetry system was running efficiently until the end of the 2018 LHC run. Several problems with readout electronics occurred in October. Most of them were fixed immediately, and the effect on data was minimal. Two ECAL ADCs and a PRS Control Board failed in October because of an incident with the cooling system. They were replaced by a spare PRS board the same day. Furthermore, one SPD Very Front End (VFE) board failed and as it is not possible to replace this kind of board without opening the detector, the 64 SPD cells served by this board remained non-operational until the end of the 2018 run. The corresponding area at the detector is visible in the Fig. 3. In addition, there are a few dead and noisy cells in the ECAL and HCAL. The CALO Upgrade will consist in removing the SPD and PS detectors and the lead converter, and replacement of the ECAL and HCAL electronics. Since the beginning of LS2, we have been working on preparations for the PS and SPD dismantling. The SPD and PS VFEs are partially removed. The production of storage cradles for the detector modules and lead converter planes is ongoing. Figure 2 shows the test of the storage cradle for the lead converter. The dismantling will start in the middle of April.

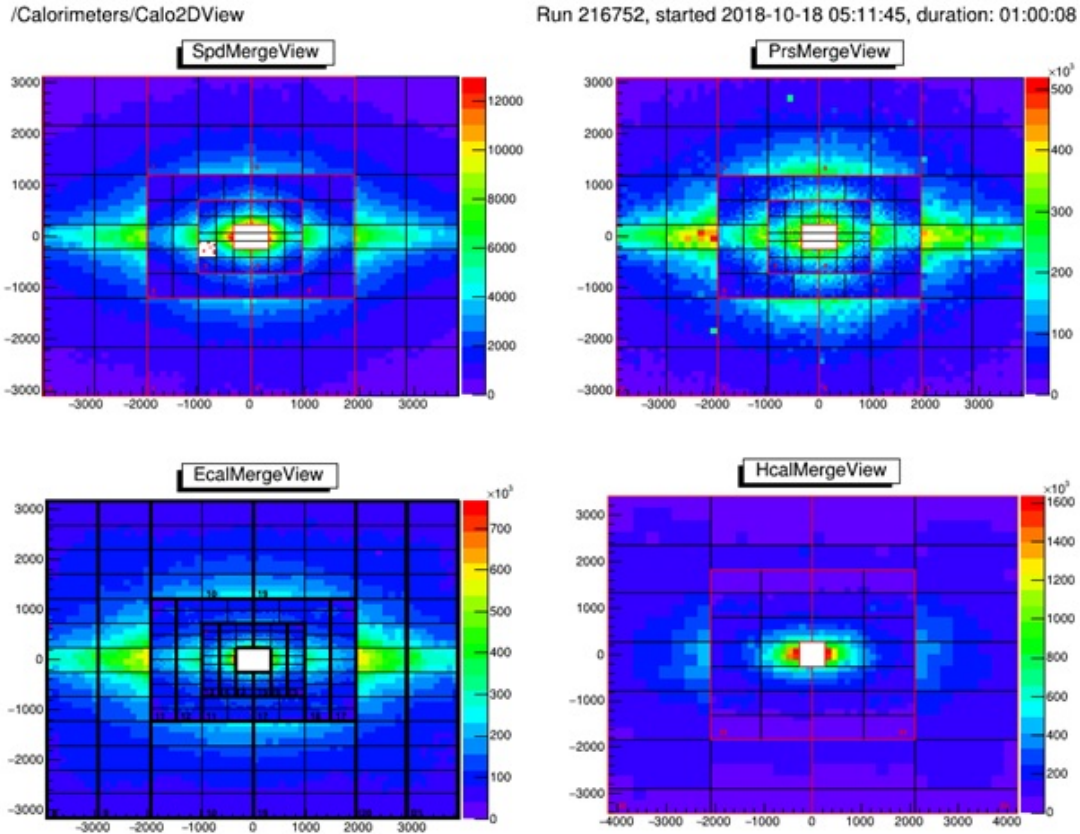


Figure 3: Merged view of CALO detectors, 200k events. At the SPD front face, the area corresponding to the broken VFE is visible.

2.6 Muon system

During the last months of the 2018 data taking, the Muon Detector has operated in a very stable manner, with all station efficiencies exceeding 99%. This is well illustrated in Fig. 5, where the track density (number of tracks per surface unit) on all the five stations is shown. Only a couple of minor local inefficiency spots were present in the detector, with a negligible impact on the overall detector performance.

Given the very high number of MWPCs (1380, with four active gas gaps each), it is crucial to maintain all the MWPCs in optimal working conditions to reach this level of efficiency. This is obtained by continuously monitoring their currents and optimizing the HV for each gap, to minimize current trips and subsequent noise generation.

Thanks to this continuous optimization process during the last months of data taking, the number of gaps suffering from HV trips in presence of beam was only 56 (out of $\simeq 5000$ gaps, so about 1%). This is the same level as measured during 2017 and a factor of two less than in 2016, which denotes a positive trend in the



Figure 4: Load tests of the storage cradle for the lead converter.

operation of the detector.

These results represents a remarkable success, for a system made of 1380 chambers and more than 122000 front-end channels (and after almost ten years of operation). Another very important fact, is that no ageing effects are visible so far in any region of the detector. This is very reassuring, as most of the chambers will be operated up to the end of Run 4 (apart from M1 station, which is being dismantled now). In addition, a well established HV training procedure is applied to all problematic chambers during each winter shutdown. This guaranteed so far a very smooth data taking operation of the detector during the subsequent data taking period.

Another crucial ingredient to ensure a succesful operation during the forthcoming years, is a careful preparatory work of an adequate stock of spare detectors and Front End electronic boards (FEBs). This task is accomplished in the muon experimental area at building 169, where the recently produced spare MPWCs are being dressed with front-end electronics. Those chambers are tested together with all of the others from old productions, for a total stock of about 150 spare MWPCs for stations M2 to M5, $\sim 15\%$ of the installed chambers.

At present, the dismantling of the most upstream muon station M1 and the prepa-

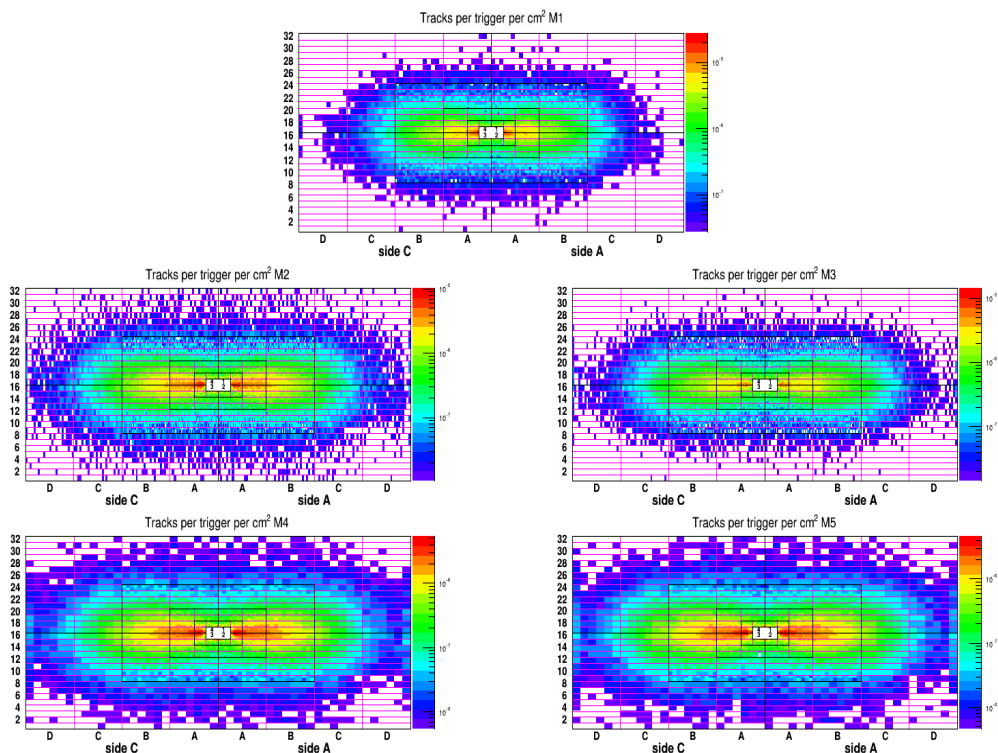


Figure 5: Track density distribution in the 5 Muon stations, as measured at the end of Run2.

ration for the new Off Detector Electronics installation is ongoing. From the station M1, several recovered components such as the FEBS, crates and HV boards, will further increase the number of spare parts to guarantee a smooth operation of the detector in the forthcoming years.

2.7 Forward shower counters (HeRSChEL)

Data taking with the HERSCHEL sub-detector proceeded smoothly during the final part of the 2018 run and information from the detector continued to be employed at every level of the trigger for low multiplicity hadronic events. The use of HERSCHEL continued to grow offline, and Autumn saw the publication of the first paper to use HERSCHEL information in JHEP [10 (2018) 167]. The machinery to enable analysts to generate easily a single HERSCHEL ‘activity metric’ has continued to be developed, and configuration of the metric for non-proton-proton data-taking has begun in line with the growing interest in using HERSCHEL for analysis of proton-lead and lead-lead data.

In the first weeks of January 2019 the counters (PMT and scintillator units) were unmounted and removed from the tunnel and, after RP measurements, were subsequently disassembled on the surface. The programme for removal of the

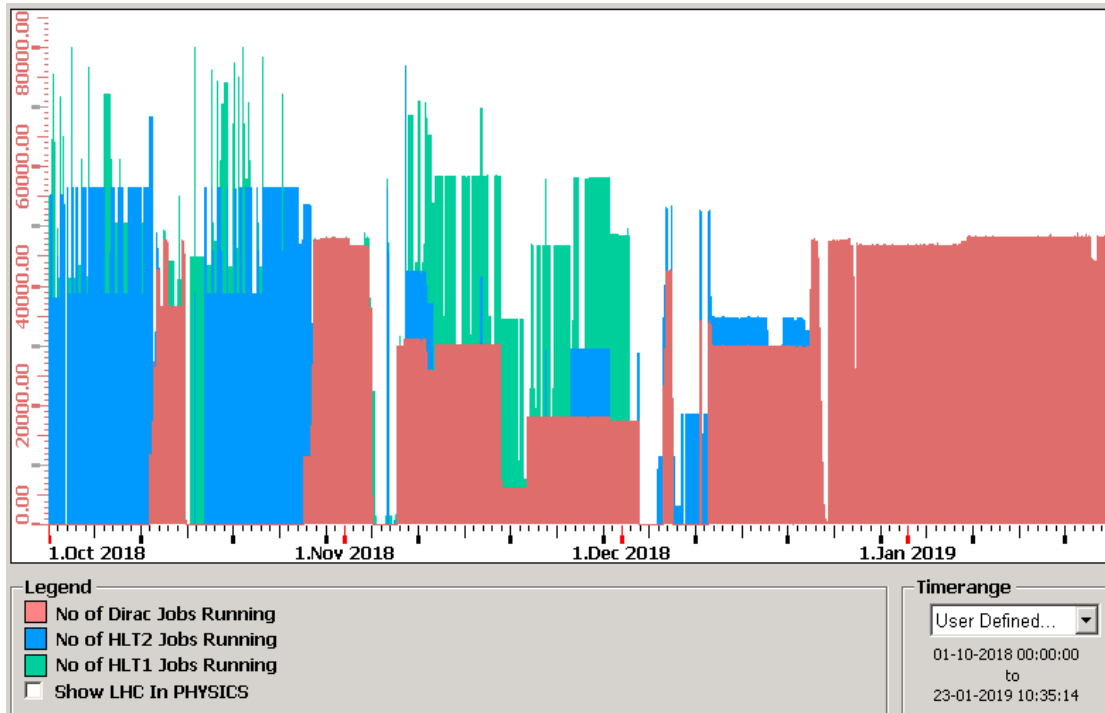


Figure 6: Number of processes running on the HLT farm.

remaining detector infrastructure is developing, with the moveable frames expected to be removed during March/April.

2.8 Online system

Since the last report the Online system successfully acquired the Heavy Ion data and all data was processed through the HLT trigger shortly before Christmas. During HLT2 processing of the Ion data Monte-Carlo production was running in parallel and since 22 December, the entire Farm is dedicated to MC production. The number of jobs is limited by memory usage and is typically 1 job less than the number of cores in the nodes, Fig. 6. During the long cooling maintenance end 2019 the MC production will be interrupted and the farm nodes moved to the new Data Center on the surface. After that, the MC production will be resumed.

3 Operations

In 2018, LHCb recorded a total integrated luminosity of 2.2 fb^{-1} with proton-proton collisions at a centre-of-mass energy of 13 TeV, with a global efficiency of about 90%. Since 2011, LHCb collected 9.1 fb^{-1} of integrated luminosity with proton-proton collisions. The last few weeks of 2018 were dedicated to the Pb-Pb collisions at a lower centre-of-mass energy of 5.02 TeV. LHCb collected a total

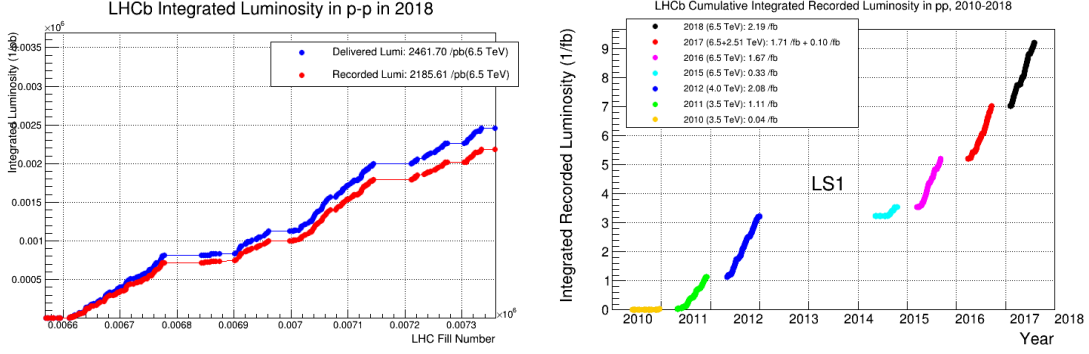


Figure 7: Delivered and recorded integrated luminosity for the 2018 proton-proton run (on the left) and for the full LHC data taking period since 2011 (on the right).

E (Z TeV)	$\sqrt{s_{NN}}$			
	pp $\sqrt{s}=2E$	208Pb-p $\sqrt{s}=2E\sqrt{r}$	208Pb-208Pb $\sqrt{s}=2Er, r=82/208$	$^{129}\text{Xe}-^{129}\text{Xe}$ $\sqrt{s}=2Er, r=54/129$
1.38	2.76 ²⁰¹³			
2.51	5.02 ^{2015, 2017}			
3.5	7 ²⁰¹¹		2.76 ²⁰¹⁰ LHCb off	
4.0	8 ²⁰¹²	5.02 ^{2013, 2016}		
6.37			5.02 ^{2015, 2018}	
6.5	13 ²⁰¹⁵⁻²⁰¹⁸	8.16 ²⁰¹⁶		5.44 ²⁰¹⁷

Figure 8: The table summarizes the LHC beam energy and the centre-of-mass energy of the data taken by the LHCb experiment during Run 1 and Run 2 data taking.

integrated luminosity of about 0.2 nb^{-1} . Figure 7 summarises the delivered and recorded luminosity for the proton-proton collisions in 2018 and for the full period since 2011. During Run 1 and Run 2, LHCb took data with proton and ions collisions at several centre-of-mass energy. Table 8 summarizes the beam energy and the centre-of-mass energy of the data taken by the experiment.

The SMOG system (System to Measure the Overlap integral with Gas) is used to inject gas into the VELO detector region, to act as a fixed target for the LHC beam. In 2018, the experiment took data injecting Ne gas during Pb-Pb runs and collected both collision and fixed-target events in parallel. Since 2015, LHCb used this system to collect collisions between the LHC proton beam and different types of gas. Figure 9 summarises the collisions taken with SMOG system since 2015.

3.1 Trigger

In the LHCb experiment, the hardware trigger (L0) is followed by two-stage software trigger. In Run 2 data taking strategy, after the first trigger stage (HLT1)

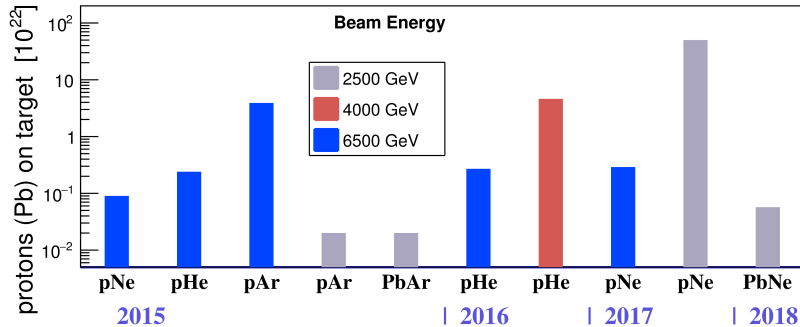


Figure 9: Number of protons on target (injected gas), for all type of gas used to collect beam-gas collision taken by LHCb experiment since 2015. The different colours indicate the beam energy.

the data are stored on disk buffers of the online-farm with a capacity of about 11 PB. The HLT1 processing is performed during the fill, while the second software trigger stage (HLT2) is processed asynchronously during the fill at a lower rate of about 30 kHz and out of the fill at a rate of about 90 kHz. The deferred HLT2 processing allows the evaluation of the real-time alignment and calibration of the detector, before the data processing in the second stage of the software trigger.

During 2018, LHCb ran with a stable trigger configuration during the full year. As in previous years, two sets of HLT1 selections were prepared: a tight configuration with an output rate of 90 kHz, and a loose configuration with an output rate of 105 kHz. The loose selection was used from the beginning of the data taking, with the strategy to swap to the tight configuration if needed to avoid overfilling the disk buffers. The risk of overfilling the disks was evaluated by monitoring the disk status and by evaluating the projection to the end of the data taking. The loose selection was used for the entire year. Figure 10 shows the projection of the disk buffer usage evaluated for several toy models at the beginning of 2018 and the effective usage during the entire 2018 data taking.

3.2 Use of the online-farm for Monte Carlo productions

The simulation samples are one of the key elements for the validation of the physics measurements and to evaluate the associated errors. Very large simulation productions are needed for achieving the high precision measurements requested by the ambitious LHCb physics programme. These requests are constantly growing and are using the largest fraction ($\sim 85\%$) of the total computing power. Efforts are ongoing in the LHCb experiment to provide multiple options for simulating events in a faster way, in particular when high statistics is needed. Two examples are to simulate only partially the detector and to simulate only particles from the signal decay and re-use the underlying event.

To profit of the resource available and to boost the Monte Carlo production, the

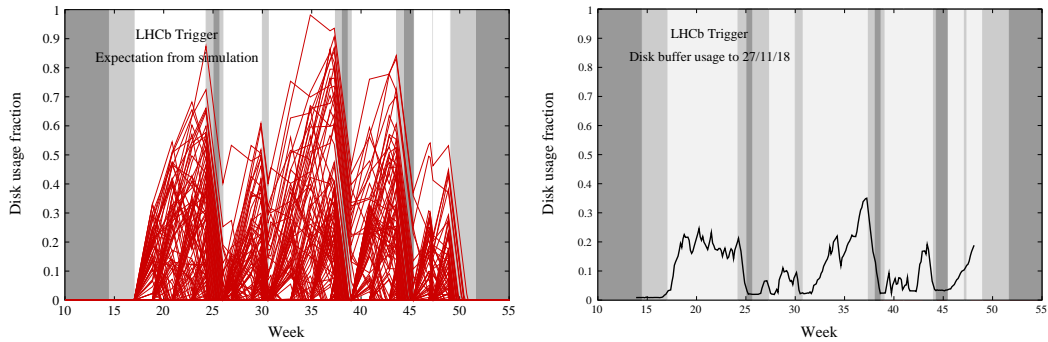


Figure 10: On the left: projection for the disk buffer usage for the 2018 data taking for several toy models based on the assumption of a 50 % LHC availability (red lines). On the right: evolution of the disk usage in 2018.

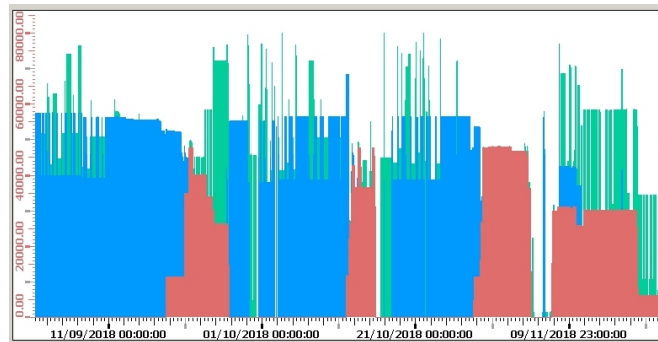


Figure 11: The number of jobs run on the online-farm during the last months of 2018: red histograms indicate Monte Carlo jobs, green histograms the HLT1 jobs, blue histograms the HLT2 jobs.

online-farm is used for simulation jobs when it is not used for the trigger processing (e.g. YETS, technical stops or machine development periods). In 2018, during the Pb-Pb data taking, it was possible to profit from about half of the online-farm to produce Monte Carlo samples in parallel to the normal HLT processing. Figure 11 shows the jobs running on the online farm for the last part of the year. During YETS, about 50% of Monte Carlo samples were produced on the online-farm.

3.3 Real-time analyses

The real-time alignment and calibration was implemented at the beginning of Run 2 and improved in the following years. This procedure allows to profit from the fully aligned and calibrated detector already in the software trigger. Thanks to this and together with the possibility to run the full reconstruction, the second stage of the software trigger can profit from the best performance both for the tracking and particle identification and maximise the selection efficiency.

The real-time alignment is evaluated on a fill-by-fill basis and is updated when a

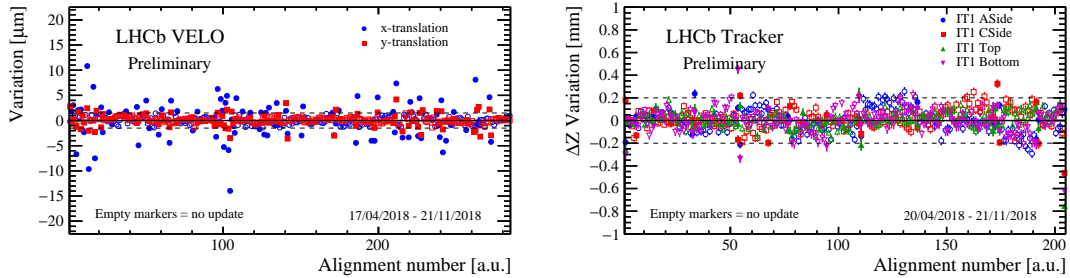


Figure 12: Variation of the VELO (on the left) and of the IT boxes (on the right) alignment constants for the entire 2018 data taking. The dashed lines indicate the minimum variation at which an alignment difference is considered significant. Each point shows the variation of the alignment parameter with respect to the constants used. The full markers indicate when an alignment update was needed.

significant variation is observed. This includes the alignment of the vertex detector, the tracker system, the muon chambers and the RICH mirrors. The calibration is evaluated and updated on a run-by-run basis for the RICH detector and for the global time calibration of the OT, and on a monthly basis for the electromagnetic calorimeter. In 2018, all the alignment and calibration jobs automatically and smoothly run. The observed variation for all the sub-systems were as expected. Figure 12 shows the relative variation of some of the VELO and IT alignment constants with respect to the previous alignment update for the entire 2018.

The real-time alignment and calibration is a key element to have a physics analysis performed directly on the trigger-reconstructed candidates with the same performance as the ones on the offline reprocessing data. These events are saved on a dedicated stream, the so-called Turbo stream. The possibility to select the physics objects to be stored for each analysis allows us to reduce the resources required with respect to the full stream without limiting the physics analyses using it.

As in previous years, the calibration stream is used to measure efficiencies and other performance metrics directly from the data. Events in the calibration stream contain the persisted trigger candidates in addition to the raw sub-detector data. This stream is used for the evaluation of the tracking efficiency and for the charged particle identification calibration.

3.4 Computing

The usage of computing resources for 2018 [2], the estimates of computing requirements for 2020 and a preview of requests for 2021 onwards [3], are discussed in detail in separate documents. The LHCb Computing Model for the Upgrade era is presented in [4].

4 Physics results

Since the last RRB report, the LHCb collaboration has submitted 19 new papers, for a total of 466 publications at the time of writing. A summary of these is given in Table 1. A further 14 papers are being processed by the LHCb Editorial Board and are close to submission. In the following, some selected results from recent publications are highlighted.

4.1 CP violation and mixing

LHCb continues to pursue a broad programme of analyses studying CP violation and mixing in the heavy quark sector. This ranges from CKM metrology, aiming to uncover internal inconsistencies in the Standard Model picture of quark couplings through a combination of precision measurements, to searches for New Physics and null tests of the SM through sensitive probes like B_s^0 mixing, to investigation of the large local CP asymmetries observed in multibody charmless b-hadron decays, to studies of mixing and ever-more sensitive searches for CP violation in charm.

Since the last RRB report, LHCb has published two new measurements in this area of charm physics. The first (LHCb-PAPER-2018-038 [5]) concerns the charm mixing parameter y_{CP} , which is related to the ratio of the D^0 lifetime measured with decays to CP -even final states (in this analysis, K^+K^- and $\pi^+\pi^-$) and the effective lifetime measured with decays to CP -mixed final states ($K^-\pi^+$). In the limit of CP conservation, the mass eigenstates and the CP eigenstates are aligned and y_{CP} becomes identical to the mixing parameter $y \equiv (\Gamma_1 - \Gamma_2)/(\Gamma_1 + \Gamma_2)$ (where Γ_1 and Γ_2 are the widths of the two mass eigenstates). Conversely, if CP is violated then, in general, $y \neq y_{CP}$. A measurement of y_{CP} is thus a constraint on both mixing and indirect CP violation in charm. LHCb measured y_{CP} with 3 fb^{-1} of data from Run 1, obtaining values¹ of $(0.63 \pm 0.15 \pm 0.11)\%$ with $D^0 \rightarrow K^+K^-$ and $(0.38 \pm 0.28 \pm 0.15)\%$ with $D^0 \rightarrow \pi^+\pi^-$. The two measurements are consistent, and their average is $y_{CP} = (0.57 \pm 0.13 \pm 0.09)\%$. This is consistent with, and as precise as, the current world-average value for y_{CP} : $(0.84 \pm 0.16)\%$ [6]. It is also consistent with the world-average value for y , $(0.62 \pm 0.07)\%$ [6], and therefore with the hypothesis of no indirect CP violation.

The second charm result in this area, LHCb-PAPER-2018-041 [7], is a search for direct CP violation in the four-body charm decay $D^0 \rightarrow K^+K^-\pi^+\pi^-$. Singly Cabibbo-suppressed decays such as this are particularly sensitive to CP violation in charm. While several previous LHCb analyses have searched for CPV in charm in a model-independent way, such as by measuring asymmetries in bins of phase space, this study uses an amplitude analysis. This approach is more complex but should ultimately have better sensitivity and allows for a more concrete interpretation of the results. It also generates useful information on the amplitude structure that may be used, for example, in future time-dependent studies of $D^0 \rightarrow K^+K^-\pi^+\pi^-$.

¹Unless otherwise stated, where two or more uncertainties are quoted the first is statistical and the second systematic.

Table 1: Papers submitted for publication since the previous RRB report.

PAPER-2018-034	Evidence for an $\eta_c(1S)\pi^-$ resonance in $B^0 \rightarrow \eta_c(1S)K^+\pi^-$ decays	19 Sep
PAPER-2018-032	Observation of two resonances in the $\Lambda_b^0\pi^\pm$ systems and precise measurement of $\Sigma_b^{*\pm}$ and $\Sigma_b^{*\pm}$ properties	20 Sep
PAPER-2018-033	Measurement of the branching fractions of the decays $D^+ \rightarrow K^-K^+K^+$, $D^+ \rightarrow \pi^- \pi^+ K^+$ and $D_s^+ \rightarrow \pi^- K^+ K^+$	07 Oct
PAPER-2018-038	Measurement of the charm-mixing parameter y_{CP}	16 Oct
PAPER-2018-035	Study of Υ production in $p\text{Pb}$ collisions at $\sqrt{s_{NN}} = 8.16$ TeV	17 Oct
PAPER-2018-023	First measurement of charm production in fixed-target configuration at the LHC	18 Oct
PAPER-2018-041	Search for CP violation through an amplitude analysis of $D^0 \rightarrow K^+K^-\pi^+\pi^-$ decays	20 Nov
PAPER-2018-037	Search for the rare decay $B^+ \rightarrow \mu^+\mu^-\mu^+\nu_\mu$	14 Dec
PAPER-2018-042	Study of the $B^0 \rightarrow \rho(770)^0 K^{*}(892)^0$ decay with an amplitude analysis of $B^0 \rightarrow (\pi^+\pi^-)(K^+\pi^-)$ decays	17 Dec
PAPER-2018-036	Measurement of the branching fraction and CP asymmetry in $B^+ \rightarrow J/\psi p^+$ decays	17 Dec
PAPER-2018-043	Model-independent observation for exotic contributions to $B^0 \rightarrow J/\psi K^+\pi^-$ decays	17 Jan
PAPER-2018-040	Observation of the doubly Cabibbo-suppressed decay $\Xi_c^+ \rightarrow p\phi$	18 Jan
PAPER-2018-047	Measurement of the mass and production rate of Ξ_b^- baryons	21 Jan
PAPER-2017-041	Measurement of the ratio of branching fractions of the decays $\Lambda_b^0 \rightarrow \psi(2S)\Lambda$ and $\Lambda_b^0 \rightarrow J/\psi\Lambda$	06 Feb
PAPER-2018-046	Observation of $B_{(s)}^0 \rightarrow J/\psi p\bar{p}$ decays and precision measurements of the $B_{(s)}^0$ masses	14 Feb
PAPER-2018-048	Measurement of B^+ , B^0 and Λ_b^0 production in $p\text{Pb}$ collisions at $\sqrt{s_{NN}} = 8.16$ TeV	14 Feb
PAPER-2018-039	Dalitz Plot analysis of the $D^+ \rightarrow K^-K^+K^+$ decay	15 Feb
PAPER-2018-050	Measurement of b -hadron fractions in 13 TeV pp collisions	18 Feb
PAPER-2018-045	Amplitude analysis of $B_s^0 \rightarrow K_S^0 K^\pm \pi^\mp$ decays	21 Feb

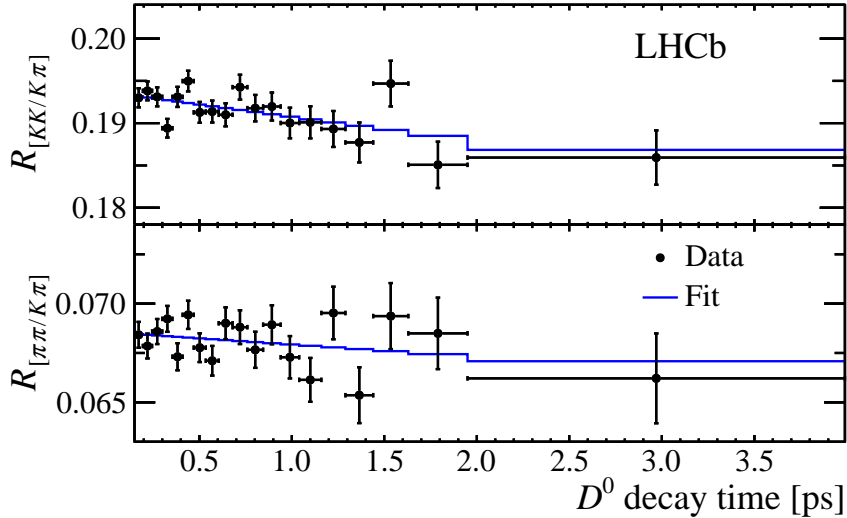


Figure 13: The acceptance-corrected ratio of the signal yields (top) $D^0 \rightarrow K^- K^- / D^0 \rightarrow K^- \pi^+$ and (bottom) $D^0 \rightarrow \pi^- \pi^+ / D^0 \rightarrow K^- \pi^+$ as a function of D^0 decay time, with a fit projection taking into account charm mixing overlaid. The variation with decay time is related to the mixing parameter y_{CP} , and is consistent between the two decay modes. From LHCb-PAPER-2018-038 [5]).

With a sample of more than 160k signal events from Run 1, the analysis measures the CP asymmetries of numerous amplitudes but finds all of them to be consistent with zero and thus does not observe any CP violation.

Time-integrated searches for CP violation were also performed in several different multibody decay modes of b hadrons. We consider first LHCb-PAPER-2018-042 [8], which again uses the technique of amplitude analysis, this time to study $B^0 \rightarrow \pi^+ \pi^- K^+ \pi^-$. The full phase space of a 4-body B^0 decay is large, and this analysis focuses on the region in the vicinity of $B^0 \rightarrow \rho(770)^0 K^*(892)^0$ —specifically, $300 < m(\pi^+ \pi^-) < 1100 \text{ MeV}/c^2$ and $750 < m(K^+ \pi^-) < 1200 \text{ MeV}/c^2$. As well as the $\rho(770)^0$ and $K^*(892)^0$, the amplitude model includes other resonances (*e.g.* the $f_0(890)$, w , $K_0^*(1430)^0$) and broader S -wave contributions. Using 3 fb^{-1} of data from Run 1, results are reported in the form of CP -averaged fit fractions, CP asymmetries for each amplitude, and relative phases between the amplitudes (including CP averages and differences). The CP -averaged longitudinal polarisation fraction for $B^0 \rightarrow \rho(770)^0 K^*(892)^0$ is found to be quite small, $0.164 \pm 0.015 \pm 0.022$, and to have a large CP asymmetry with significance in excess of 5σ .

The process $B^+ \rightarrow J/\psi \rho^+$, with $J/\psi \rightarrow \mu^+ \mu^-$ and $\rho^+ \rightarrow \pi^+ \pi^0$, is also studied with 3 fb^{-1} of data from Run 1, as reported in LHCb-PAPER-2018-036 [9] In this case, though, the decays are treated as quasi-two-body. The signal yield is determined with a two-dimensional fit to $m(J/\psi \pi^+ \pi^0)$ and $m(\pi^+ \gamma \gamma)$, allowing the non-resonant $B^+ \rightarrow J/\psi \pi^+ \pi^0$ component to be separated and removed. After correc-

tion for efficiency, the branching fraction is measured relative to the normalisation mode $B^+ \rightarrow J/\psi K^+$ and found to be $\mathcal{B}(B^+ \rightarrow J/\psi \rho^+) = (3.81_{-0.24}^{+0.25} \pm 0.35) \times 10^{-5}$. The CP asymmetry is measured to be $\mathcal{A}_{CP}(B^+ \rightarrow J/\psi \rho^+) = -0.045_{-0.057}^{+0.056} \pm 0.008$ and is consistent with zero and with the corresponding measurement of $B^0 \rightarrow J/\psi \rho^0$ [10], as expected from isospin symmetry. Precise theory predictions for this asymmetry are not available; rather, the object of the measurement is to help constrain penguin effects on $B_s^0 \rightarrow J/\psi \phi$.

4.2 Rare decays

Another major arm of LHCb’s physics programme is the search for physics beyond the Standard Model through the search for, and precise measurement of, rare decay processes. One new result was published in this area since the last RRB report, namely a search for $B^+ \rightarrow \mu^+ \mu^- \mu^+ \nu_\mu$ with 4.7 fb^{-1} of data from 2011–2016 (LHCb-PAPER-2018-037 [11]). This process is allowed but suppressed in the SM, with contributions from $B^+ \rightarrow \mu^+ \nu_\mu \gamma^*$ and $B^+ \rightarrow \mu^+ \nu_\mu V$, where the virtual photon γ^* or the vector meson resonance V decays to a pair of muons. The branching fraction for the process is difficult to calculate; a theoretical prediction of around 1.3×10^{-7} based on vector-meson dominance exists [12]. However, the LHCb analysis found no signal (see Fig. 14) and set a more stringent upper limit, of $\mathcal{B}(B^+ \rightarrow \mu^+ \mu^- \mu^+ \nu_\mu) < 1.6 \times 10^{-8}$ at the 95% confidence level. This result will no doubt stimulate further theoretical work in this area. It is also of interest because $B^+ \rightarrow \mu^+ \mu^- \mu^+ \nu_\mu$ is an important background to $B^+ \rightarrow \mu^+ \nu_\mu$, so the strict limit bodes well for future studies of this mode at Belle-II.

4.3 Hadronic physics: production, spectroscopy, decays

LHCb has a substantial programme of hadronic physics, including studies of production rates, branching fractions and decays (including amplitude analysis of multi-body decays), and spectroscopy.

4.3.1 Production

Beginning with production, LHCb has published two recent results. First, there is a measurement of b -hadron production fractions in 13 TeV pp collisions (LHCb-PAPER-2018-050 [13]). These quantify the production of B_s^0 and of Λ_b^0 in the LHCb kinematic acceptance, normalised to the sum of B^+ and B^0 production, and are essential for determining the absolute branching fractions of decay modes of these hadrons (*e.g.* in $B_s^0 \rightarrow \mu^+ \mu^-$). A relative production fraction of $f_s/(f_u + f_d) = 0.122 \pm 0.006$ is obtained for B_s^0 , and $f_{\Lambda_b^0}/(f_u + f_d) = 0.259 \pm 0.018$ for Λ_b^0 ; the substantial rate of heavy baryon production at the LHC is seen clearly, and is found to depend strongly on the hadron p_T .

Second, LHCb carried out measurements of the production rate of Ξ_b^- baryons at $\sqrt{s} = 7, 8,$ and 13 TeV in the kinematic region ($2 < \eta < 6$ and $p_T < 20 \text{ GeV}$) in

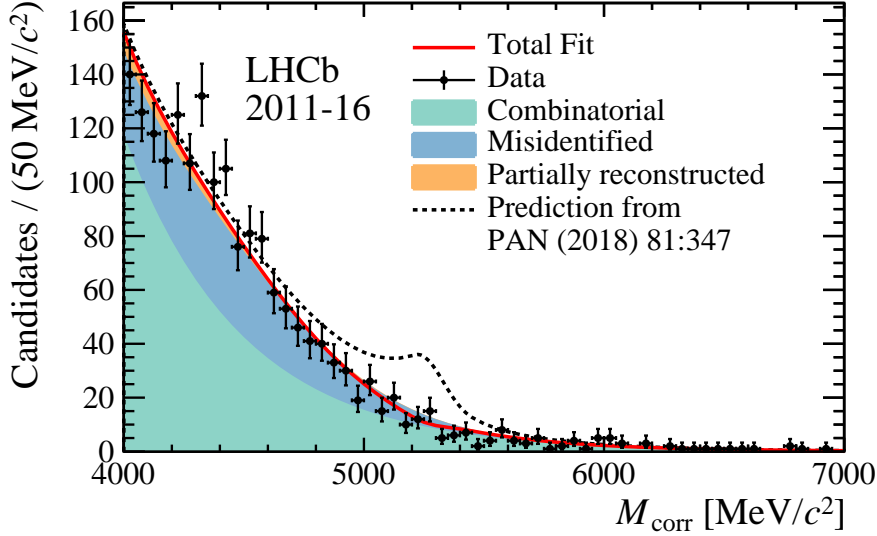


Figure 14: Distribution of reconstructed $m(\mu^+\mu^-\mu^+\nu_\mu)$, corrected for the missing neutrino momentum. The fit has components for (green) combinatorial background, (blue) misidentified candidates and (orange) partially reconstructed candidates. The total of the signal plus background is shown as the solid red line. No signal is found (the central value of the yield is negative). The dashed line shows how the total under an alternative hypothesis taking the signal yield from a theory prediction [12]. From LHCb-PAPER-2018-037 [11]).

LHCb-PAPER-2018-047 [14]. The Ξ_b^- are observed via the decay $\Xi_b^- \rightarrow J/\psi \Xi^-$, and the production rate is measured relative to $\Lambda_b^0 \rightarrow J/\psi \Lambda$. The ratio of branching fractions $\mathcal{B}(\Xi_b^- \rightarrow J/\psi \Xi^-)/\mathcal{B}(\Lambda_b^0 \rightarrow J/\psi \Lambda)$ has not been measured, but can be estimated from $SU(3)$ flavour symmetry. On this basis, the production ratio $f_{\Xi_b^-}/f_{\Lambda_b^0}$ is estimated to be $(6.7 \pm 0.5 \pm 0.5 \pm 2.0)\%$ at $\sqrt{s} = 7, 8$ TeV and $(8.2 \pm 0.7 \pm 0.6 \pm 2.4)\%$ at 13 TeV, where the third uncertainty is that associated with $SU(3)$ breaking. In the same analysis, a measurement of the mass difference between the Λ_b^0 and Ξ_b^- states is made. Combined with previous measurements of the Λ_b^0 mass, this allows the most precise determination of the Ξ_b^- mass to be made: $m(\Xi_b^-) = 5796.70 \pm 0.39 \pm 0.15 \pm 0.17$ MeV/ c^2 , where the third uncertainty is due to the precision on the world-average Λ_b^0 mass.

4.3.2 Spectroscopy

As the previous measurement illustrates, LHCb is able to measure the properties of hadronic states with precision. As well as ground states, LHCb has also reported results on several resonances since the last RRB report. In LHCb-PAPER-2018-034 [15], LHCb carried out an amplitude analysis of the decay process $B^0 \rightarrow \eta_c(1S)K^+\pi^-$, $\eta_c(1S) \rightarrow p\bar{p}$, using data from 2011–2016. As well as a measurement

of the branching fraction, $\mathcal{B}(B^0 \rightarrow \eta_c(1S)K^+\pi^-) = (5.73 \pm 0.24 \pm 0.13 \pm 0.66) \times 10^{-4}$, an amplitude analysis of the decay is performed. Here the classic Dalitz plot formalism with two degrees of freedom can be used, since the final state $\eta_c(1S)K^+\pi^-$ consists of three pseudoscalar mesons. A model which contains no exotic resonances (*i.e.* in which the only dynamic structure comes from $K^+\pi^-$ resonances) is unable to describe the data well. However, when an exotic $Z_c \rightarrow \eta_c(1S)\pi^-$ resonance is added to the amplitude model, the agreement with data improves. Taking into account the look-elsewhere-effect but ignoring systematic uncertainties, the improvement in fit quality corresponds to a statistical significance of 4.8σ . When variations due to systematic effects are considered, the significance is reduced but remains at or above 3.2σ . The analysis therefore presents evidence but not an observation of the presence of exotic structure. In the best-fit model, the exotic structure $Z_c(4100)^-$ has mass $4096 \pm 20 \text{ MeV}/c^2$ and width $152 \pm 58 \text{ MeV}$.

In another analysis, this time of $B^0 \rightarrow J/\psi K^+\pi^-$ decays in LHCb-PAPER-2018-043 [16], a related approach was used to demonstrate with high significance that exotic contributions must be present using Run 1 data. In this analysis, the strategy used is to divide the phase space into narrow slices of $m(K^+\pi^-)$. If only kaon resonances are present then, within a given slice, the angular distribution in each slice can be expressed as an expansion in a series of basis functions up to a finite order, with the number of terms contributing related to the highest-spin kaon resonance present. This is assumed to be $J \leq 2$ for $1085 < m(K^+\pi^-) < 1265 \text{ MeV}/c^2$ and $J \leq 3$ for $1265 < m(K^+\pi^-) < 1445 \text{ MeV}/c^2$. Thus, with minimal assumptions, a complete model for all possible non-exotic amplitudes can be fitted to the data without requiring prior knowledge of the number and nature of the contributing kaon resonances—this forms the null hypothesis. Exotic contributions in $m(J/\psi \pi^-)$ or $m(J/\psi K^+)$ would cut across the Dalitz-like plot and generate higher-order terms in $m(K^+\pi^-)$. Allowing such contributions (parameterised in the same angular basis with functions up to $J = 15$) greatly improves the agreement with data, with a statistical significance in excess of 6σ (allowing for systematic effects). This establishes the presence of exotic contributions in $B^0 \rightarrow J/\psi K^+\pi^-$. It does not establish their nature; although suggestive structures at $m(J/\psi \pi^-)$ of 4200 and 4600 MeV/c^2 are seen, a proper study will require a future amplitude analysis.

Lastly, in LHCb-PAPER-2018-032 [17] LHCb reported the first observation of two Σ_b resonances in the $\Lambda_c^+\pi^-$ final state using the Run 1 data (see Fig. 15). These two resonances form two states of an isotriplet. In addition, the analysis made significantly improved measurements of the masses and widths of the lower states Σ_b^\pm and $\Sigma_b^{*\pm}$. The new states are measured to have masses of $m(\Sigma_b(6097)^-) = 6098.0 \pm 1.7 \pm 0.5 \text{ MeV}/c^2$ and $m(\Sigma_b(6097)^+) = 6095.8 \pm 1.7 \pm 0.4 \text{ MeV}/c^2$, and widths of $28.9 \pm 4.2 \pm 0.9 \text{ MeV}$ and $31.0 \pm 5.5 \pm 0.7 \text{ MeV}$, respectively. The spin-parity assignments are not measured—this is not straightforward for inclusive production—and will require further investigation.

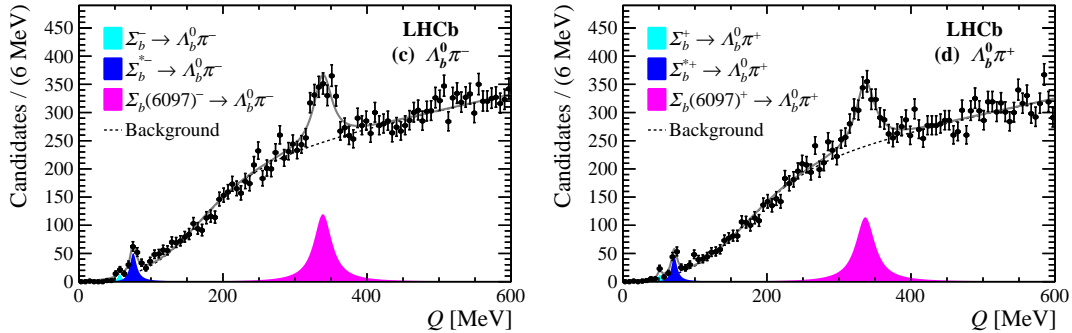


Figure 15: Distributions of $m(\Lambda_b^0\pi^-)$ and $m(\Lambda_b^0\pi^+)$ after selection, as reported in LHCb-PAPER-2018-032 [17]). The resonance $\Sigma_b(6097)^-$ (magenta) is clearly visible. The known resonances Σ_b and Σ_b^* are visible at the left (light, dark blue) but are strongly suppressed by the p_T cut on the pion.

4.3.3 Amplitude analysis

We have already seen that amplitude analysis techniques play an important role in numerous LHCb measurements, from studies of CP violation and mixing to studies of resonances within multibody decays. LHCb has also submitted papers in which the amplitude analysis itself is the primary output, with a view to improving our ability to understand and model multibody decays. Each of the two papers described below contains the first amplitude analysis of a particular decay mode. In LHCb-PAPER-2018-039 [18], LHCb presented the first amplitude analysis of the doubly Cabibbo-suppressed decay $D^+ \rightarrow K^+K^-K^+$, using 2 fb^{-1} of data from Run 1. Despite the suppression, the high charm cross-section at LHCb leads to a yield of roughly 100k events. Two different models are used to fit the data: one in the well-known isobar framework, and one using a phenomenological approach known as the multi-meson model [19]. The latter takes into account coupled channels and can therefore be used to make predictions for $K\bar{K} \rightarrow K\bar{K}$ scattering amplitudes from the fit to $D^+ \rightarrow K^+K^-K^+$. Both models are able to describe the data, which include a clear $D^+ \rightarrow \phi(1020)K^+$ component (at the 6–7% level) as well as a large S -wave contribution.

The first untagged, decay-time-integrated analysis of $B_s^0 \rightarrow K_S^0K^+\pi^-$ and $B_s^0 \rightarrow K_S^0K^-\pi^+$ is presented in LHCb-PAPER-2018-045 [20], using the Run 1 data. Because of the limited signal yield—roughly 900 events—the analysis is carried out without attempting to separate B_s^0 from \bar{B}_s^0 decays² An amplitude model within the isobar formalism is found to describe the data well and allows fit fractions for intermediate resonances to be measured. These are found to be consistent with branching fraction predictions. Mapping out the amplitude structure in this

²This is due to the rapid B_s^0 oscillations and the limited effective tagging efficiency at LHCb (typically several percent); it is not practical to separate the two decays with pre-upgrade statistics.

way lays the foundations for a future tagged, time-dependent study in which CP asymmetries could be measured.

4.3.4 Hadronic decays and branching fractions

As in the previous analysis, branching fractions may be measured and compared to predictions to test hadronic decay models, so as to understand how reliable their predictions may be for other processes or observables. Branching fractions may also be needed as inputs to calculations, or simply to understand how much signal will be available for future studies.

In LHCb-PAPER-2018-046 [21], data taken from 2011–2016 are used to make the first observations of the decays $B^0 \rightarrow J/\psi p\bar{p}$ and $B_s^0 \rightarrow J/\psi p\bar{p}$, and to measure their branching fractions. These are found to be $\mathcal{B}(B^0 \rightarrow J/\psi p\bar{p}) = (4.51 \pm 0.40 \pm 0.44) \times 10^{-7}$ and $\mathcal{B}(B_s^0 \rightarrow J/\psi p\bar{p}) = (3.58 \pm 0.19 \pm 0.33) \times 10^{-6}$. The B_s^0 branching fraction is particularly surprising: the naive expectation is closer to 10^{-9} [22], suggesting a large threshold enhancement which could, perhaps, be associated with an intermediate pentaquark or glueball state. In addition, because the energy release in these near-threshold decays is small, they can be used to make the most precise single measurements of the B^0 and B_s^0 meson masses. The values obtained are $m(B^0) = 5279.74 \pm 0.30 \pm 0.10 \text{ MeV}/c^2$ and $m(B_s^0) = 5366.85 \pm 0.19 \pm 0.13 \text{ MeV}/c^2$.

In LHCb-PAPER-2018-033 [23], the branching fractions of the doubly Cabibbo-suppressed decays $D^+ \rightarrow K^- K^+ K^+$, $D^+ \rightarrow \pi^- \pi^+ K^+$, and $D_s^+ \rightarrow \pi^- K^+ K^+$ are studied with the data taken in 2012. (Note that the first mode is the same one used for the amplitude analysis in LHCb-PAPER-2018-051 [24].) The BF's are obtained relative to normalisation modes:

$$\begin{aligned} \frac{\mathcal{B}(D^+ \rightarrow K^- K^+ K^+)}{\mathcal{B}(D^+ \rightarrow K^- \pi^+ \pi^+)} &= (6.541 \pm 0.025 \pm 0.042) \times 10^{-4}, \\ \frac{\mathcal{B}(D^+ \rightarrow \pi^- \pi^+ K^+)}{\mathcal{B}(D^+ \rightarrow K^- \pi^+ \pi^+)} &= (5.231 \pm 0.009 \pm 0.023) \times 10^{-3}, \\ \frac{\mathcal{B}(D_s^+ \rightarrow \pi^- K^+ K^+)}{\mathcal{B}(D_s^+ \rightarrow K^- K^+ \pi^+)} &= (2.372 \pm 0.024 \pm 0.025) \times 10^{-3}. \end{aligned}$$

Note that, despite these being doubly Cabibbo-suppressed, the measurements are not statistically limited thanks to signal yields of order 10^5 – 10^6 .

In LHCb-PAPER-2018-040 [25], another doubly Cabibbo-suppressed decay is reported with the 2012 dataset, namely $\Xi_c^+ \rightarrow p\phi$. This is the first observation of this process, and its branching fraction relative to a singly Cabibbo-suppressed control mode is measured to be: $\mathcal{B}(\Xi_c^+ \rightarrow p\phi)/\mathcal{B}(\Xi_c^+ \rightarrow pK^- \pi^+) = (19.8 \pm 0.7 \pm 0.9 \pm 0.2) \times 10^{-3}$, where the third uncertainty is due to knowledge of the $\phi \rightarrow K^+ K^-$ branching fraction.

The ATLAS collaboration has previously measured the ratio of branching fractions $\mathcal{B}(\Lambda_b^0 \rightarrow \psi(2S)\Lambda)/\mathcal{B}(\Lambda_b^0 \rightarrow J/\psi\Lambda)$ to be $0.501 \pm 0.033 \pm 0.019$; this value differs

from a theory prediction of 0.8 ± 0.1 [26] by 2.8σ , as well as differing from comparable measurements in the B^0 system. In LHCb-PAPER-2017-041 [27], this ratio of branching fractions is measured by LHCb using the Run 1 data sample. The value obtained is $\mathcal{B}(\Lambda_b^0 \rightarrow \psi(2S)\Lambda)/\mathcal{B}(\Lambda_b^0 \rightarrow J/\psi\Lambda) = 0.513 \pm 0.023 \pm 0.016 \pm 0.011$, where the third value is due to external branching fraction inputs. This value is fully consistent with the ATLAS measurement, and is more precise. It confirms the tension with the theory prediction.

4.4 Heavy-ion physics

Another aspect of the LHCb physics programme which has grown in recent years is the study of heavy-ion physics. Since the last RRB report, LHCb has published papers both with samples of p -Pb collisions (collider mode) and with samples of proton-gas collisions with the SMOG system (fixed-target mode). In LHCb-PAPER-2018-035 [28], the production cross-section for $\Upsilon(1S)$, $\Upsilon(2S)$, and $\Upsilon(3S)$ mesons is studied in proton-lead collisions at a centre-of-mass energy per nucleon of $\sqrt{s_{NN}} = 8.16$ TeV, as a function of p_T and rapidity (y^*) in the nucleon-nucleon centre-of-mass frame. LHCb's forward acceptance allows these measurements to be made both for $1.5 < y^* < 4.0$ and for $-5.0 < y^* < -2.5$ (with these two kinematic regions corresponding to events in which the proton or the lead ion is moving in the $+z$ direction). By comparing these cross-sections to equivalent quantities in pp collisions interpolated to $\sqrt{s} = 8.16$ TeV, the nuclear modification factor for ^{208}Pb can be obtained (see Fig. 16). The forward-to-backward ratio (comparing $+y^*$ to $-y^*$) and the cross-section ratios between the different $\Upsilon(nS)$ states are also computed, as is the ratio of $\Upsilon(1S)$ to non-prompt J/ψ . The results are found to be consistent with theory expectations, and show a suppression of Υ production in proton-lead collisions that is more pronounced for the excited states.

Another measurement of b -hadron production in proton-lead collisions, this time with open beauty, is performed in LHCb-PAPER-2018-048 [29]. The production cross-sections of B^+ , B^0 , and Λ_b^0 are reported as functions of p_T and y^* , and as for the previous paper the nuclear modification factors and forward-to-backward ratios are computed. The ratio of Λ_b^0 to B^0 production is also studied, and, intriguingly, is found to be consistent with that seen in proton-proton collisions within uncertainties.

Finally, in LHCb-PAPER-2018-023 [30] production of D^0 and J/ψ is studied in proton-helium and proton-argon collisions using data taken in fixed-target mode (corresponding to centre-of-mass energies per nucleon of $\sqrt{s_{NN}} = 86.6$ and 110.4 GeV). The LHCb pseudorapidity acceptance used, 2.0 – 4.6 , corresponds to a rapidity range of approximately $-2.5 < y^* < 0$. Measurements of the D^0 and J/ψ production cross-sections in this rapidity range are carried out for the $p\text{He}$ sample (for which an integrated luminosity was available); they are found to be $\sigma(J/\psi) = 652 \pm 33 \pm 42$ nb/nucleon and $\sigma(D^0) = 80.8 \pm 2.4 \pm 6.3$ μb /nucleon.

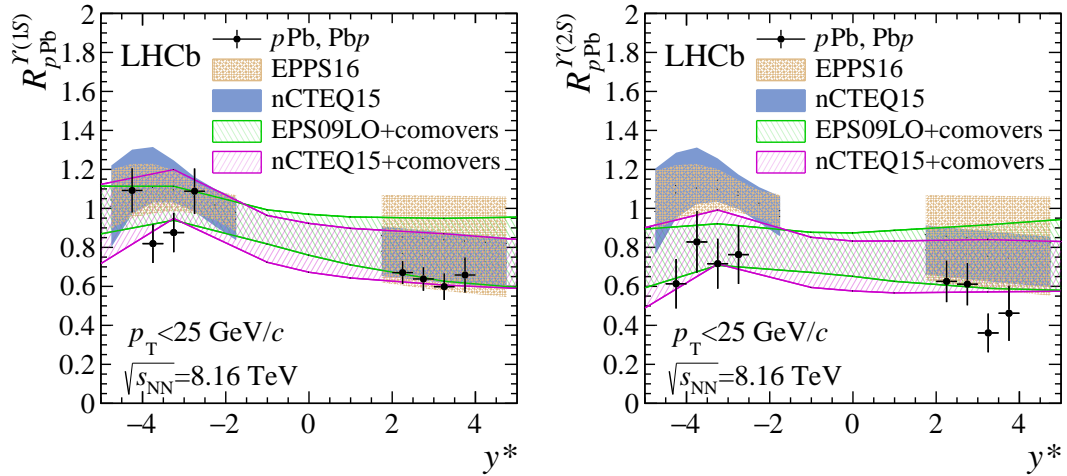


Figure 16: Nuclear modification factors of the $\Upsilon(1S)$ and $\Upsilon(2S)$ mesons as a function of rapidity y^* , integrated over p_T . The bands correspond to the theoretical predictions for the nCTEQ15 and EPPS16 nPDFs sets, and the comovers model. From an analysis of proton-lead collisions in LHCb-PAPER-2018-035 [28].

5 Financial issues

The status of the accounts is healthy and no cash flow problems are foreseen. The expenditure on the 2018 M&O Cat. A budget followed well our forecasts. A small overspending was expected and is registered. Year 2019 is expected to be balanced, despite this being the first year of LS2. The schedule follows the financial plan (M&O cat.A levels for the forthcoming LS2 and successive upgrade phase) which was finalised, submitted and approved by the Scrutiny Group and by the RRB in 2017 and 2018.

6 Collaboration matters

One group was upgraded from associate to full member, Los Alamos National Laboratory (Los Alamos, NM, USA).

References

- [1] LHCb collaboration, *Status of the LHCb upgrade*, CERN-RRB-2018-053.
- [2] C. Bozzi, *LHCb Computing Resource usage in 2018*, Tech. Rep. LHCb-PUB-2019-004. CERN-LHCb-PUB-2019-004, CERN, Geneva, 2019.
- [3] C. Bozzi, *LHCb Computing Resources: 2020 requests and preview of the subsequent years*, Tech. Rep. LHCb-PUB-2019-003. CERN-LHCb-PUB-2019-003, CERN, Geneva, 2019.
- [4] LHCb collaboration, *Computing Model of the Upgrade LHCb experiment*, Tech. Rep. CERN-LHCC-2018-014. LHCb-TDR-018, CERN, Geneva, 2018.
- [5] LHCb collaboration, R. Aaij *et al.*, *Measurement of the charm-mixing parameter y_{CP}* , Phys. Rev. Lett. **122** (2019) 011802, [arXiv:1810.06874](#).
- [6] Heavy Flavor Averaging Group, Y. Amhis *et al.*, *Averages of b -hadron, c -hadron, and τ -lepton properties as of summer 2016*, Eur. Phys. J. **C77** (2017) 895, [arXiv:1612.07233](#), updated results and plots available at <https://hflav.web.cern.ch>.
- [7] LHCb collaboration, R. Aaij *et al.*, *Search for CP violation through an amplitude analysis of $D^0 \rightarrow K^+ K^- \pi^+ \pi^-$ decays*, JHEP **02** (2019) 126, [arXiv:1811.08304](#).
- [8] LHCb collaboration, R. Aaij *et al.*, *Study of the $B^0 \rightarrow \rho(770)^0 K^*(892)^0$ mode with an amplitude analysis of $B^0 \rightarrow (\pi^+ \pi^-)(K^+ \pi^-)$ decays*, [arXiv:1812.07008](#), submitted to JHEP.
- [9] LHCb collaboration, R. Aaij *et al.*, *Measurement of the branching fraction and CP asymmetry in $B^+ \rightarrow J/\psi \rho^+$ decays*, [arXiv:1812.07041](#), submitted to EPJC.
- [10] LHCb collaboration, R. Aaij *et al.*, *Measurement of the CP-violating phase β in $\bar{B}^0 \rightarrow J/\psi \pi^+ \pi^-$ decays and limits on penguin effects*, Phys. Lett. **B742** (2015) 38, [arXiv:1411.1634](#).
- [11] LHCb collaboration, R. Aaij *et al.*, *Search for the rare decay $B^+ \rightarrow \mu^+ \mu^- \mu^+ \nu_\mu$* , [arXiv:1812.06004](#), submitted to EPJC.
- [12] A. V. Danilina and N. V. Nikitin, *Four-leptonic decays of charged and neutral B mesons within the Standard Model*, Phys. Atom. Nucl. **81** (2018) 347, [Yad. Fiz. **81** (2018) 331].
- [13] LHCb collaboration, R. Aaij *et al.*, *Measurement of b -hadron fractions in 13 TeV pp collisions*, [arXiv:1902.06794](#), in preparation.

- [14] LHCb collaboration, R. Aaij *et al.*, *Measurement of the mass and production rate of Ξ_b^- baryons*, arXiv:1901.07075, submitted to PRD.
- [15] LHCb collaboration, R. Aaij *et al.*, *Evidence for a $\eta_c(1S)\pi^-$ resonance in $B^0 \rightarrow \eta_c(1S)K^+\pi^-$ decays*, Eur. Phys. J. **C78** (2018) 1019, arXiv:1809.07416.
- [16] LHCb collaboration, R. Aaij *et al.*, *Model-independent observation of exotic contributions to $B^0 \rightarrow J/\psi K^+\pi^-$ decays*, arXiv:1901.05745, submitted to Phys.Rev.Lett.
- [17] LHCb collaboration, R. Aaij *et al.*, *Observation of two resonances in the $\Lambda_b^0\pi^\pm$ systems and precise measurement of Σ_b^\pm and $\Sigma_b^{*\pm}$ properties*, Phys. Rev. Lett. **122** (2019) 012001, arXiv:1809.07752.
- [18] LHCb collaboration, R. Aaij *et al.*, *Dalitz plot analysis of the decay $D^+ \rightarrow K^-K^+K^+$* , arXiv:1902.05884, submitted to JHEP.
- [19] R. T. Aoude, P. C. Magalhães, A. C. dos Reis, and M. R. Robilotta, *Multimeson model for the $D^+ \rightarrow K^-K^+K^+$ decay amplitude*, Phys. Rev. **D98** (2018) 056021, arXiv:1805.11764.
- [20] LHCb collaboration, R. Aaij *et al.*, *Amplitude analysis of $B_s^0 \rightarrow K_S^0 K^\pm \pi^\mp$ decays*, arXiv:1902.07955, submitted to JHEP.
- [21] LHCb collaboration, R. Aaij *et al.*, *Observation of $B_{(s)}^0 \rightarrow J/\psi p\bar{p}$ decays and precision measurements of the $B_{(s)}^0$ masses*, arXiv:1902.05588, submitted to PRL.
- [22] Y. K. Hsiao and C. Q. Geng, *$f_J(2220)$ and hadronic \bar{B}_s^0 decays*, Eur. Phys. J. **C75** (2015) 101, arXiv:1412.4900.
- [23] LHCb collaboration, R. Aaij *et al.*, *Measurement of the branching ratios of the decays $D^+ \rightarrow K^+K^-K^+$, $D^+ \rightarrow K^+\pi^+\pi^-$, $D_s^+ \rightarrow \pi^-K^-K^+$* , arXiv:1810.03138.
- [24] LHCb collaboration, R. Aaij *et al.*, *Amplitude analysis of $B^\pm \rightarrow \pi^\pm K^+K^-$ decays*, LHCb-PAPER-2018-051, in preparation.
- [25] LHCb collaboration, R. Aaij *et al.*, *Observation of the doubly Cabibbo-suppressed decay $\Xi_c^+ \rightarrow p\phi$* , arXiv:1901.06222, submitted to JHEP.
- [26] T. Gutsche *et al.*, *Polarization effects in the cascade decay $\Lambda_b \rightarrow \Lambda(\rightarrow p\pi^-) + J/\psi(\rightarrow \ell^+\ell^-)$ in the covariant confined quark model*, Phys. Rev. **D88** (2013) 114018, arXiv:1309.7879.
- [27] LHCb collaboration, R. Aaij *et al.*, *Measurement of the ratio of branching fractions of the decays $\Lambda_b^0 \rightarrow \psi(2S)\Lambda$ and $\Lambda_b^0 \rightarrow J/\psi\Lambda$* , arXiv:1902.02092.

- [28] LHCb collaboration, R. Aaij *et al.*, *Study of Υ production in pPb collisions at $\sqrt{s_{\text{NN}}} = 8.16 \text{ TeV}$* , JHEP **11** (2018) 194, [arXiv:1810.07655](#).
- [29] LHCb collaboration, R. Aaij *et al.*, *Measurement of B^+ , B^0 and Λ_b^0 production in pPb collisions at $\sqrt{s_{\text{NN}}} = 8.16 \text{ TeV}$* , [arXiv:1902.05599](#), submitted to PRD.
- [30] LHCb collaboration, R. Aaij *et al.*, *First measurement of charm production fixed-target configuration at the LHC*, [arXiv:1810.07907](#).